Particle & Particle Systems Characterization
www.particle-journal.com

Gold Nanocages as Effective Photothermal Transducers in Killing Highly Tumorigenic Cancer Cells

*Aravind Kumar Rengan, Gopal Kundu, Rinti Banerjee, and Rohit Srivastava**

Numerous gold nanostructures have the potential for photothermal therapy in cancers. Here, gold nanocages and gold nanoshells are synthesized, the sizes of which are fine-tuned for a response at 750 nm wavelength. Their photothermal therapeutic efficiency is compared at gold concentration of 100 λg mL^{-1} using a near-infrared laser (750 nm). The biocompatibility for varying concentrations of gold (1 to 100 λg mL^{-1}) is performed in a normal cell line and laser-mediated cell cytotoxicity for varying time intervals (7.5 and 10 min) is carried out in breast cancer cells. This study shows that when analyzed under similar conditions, the gold nanocages show better biocompatibility and are more efficient in near-infrared absorption and photothermal conversion in comparison with conventional gold nanoshells. When subjected to photothermal laser ablation of breast cancer cell line for 7.5 min and 10 min, the nanocages are able to induce 62.92 ± 3.25% and 96.41 ± 3.04% reduction in cell viability, respectively, in comparison to nanoshells, in which a 43.35 ± 1.91% and 79.89 ± 4.74% reduction in cell viability is observed. The current study shows that the gold nanocages can outperform gold nanoshells and effectively kill cancer cells without any significant cytotoxic effect on normal cells.

1. Introduction

Cancer nanotechnology has gained tremendous attention in the recent past owing to significant developments in the synthesis and application of potential nanomaterials that hold promise in addressing important issues related to cancer. Nanomaterials in cancer research are being explored for their efficiency both in diagnostics and in therapeutics.[1,2] Gold-based nanostructures have received great impetus in research owing to their biocompatibility and flexibility in shape, size, and surface chemistry.[3,4] They are found to have unique chemical properties enabling them to be easily functionalized to biological ligands.[5] Their optical properties have been exploited in bio-sensing,[6] photothermal transduction,[7] and in other important bio-medicine applications.[8]

Dr. A. K. Rengan, Prof. R. Banerjee, Prof. R. Srivastava
Department of Bioscience and Bioengineering
Indian Institute of Technology – Bombay
Powai, Mumbai, 400076, India
E-mail: rsrivasta@iitb.ac.in
Dr. G. Kundu
Signal Transduction Lab
National Centre for Cell Science
Ganeshkind, Pune, 411007, India

DOI: 10.1002/ppsc.201300173

During the past decade, gold nanostructures have been extensively researched for their role in photothermal therapy (PTT), which is believed to have very minimal side effects unlike the conventional modes of cancer treatment namely surgery, radiation, and chemotherapy.[9] Gold nanostructures exhibit surface plasmon resonance (SPR) due to the oscillating electron cloud, that can be tuned to a near-infrared (NIR) region of absorption. The NIR light is said to be biologically invisible, i.e., less absorbed by tissues, allowing better penetration and targeting of the nanostructures inside cells and tissues.[10] When NIR light falls on these pre-tuned nanostructures, it is absorbed and photothermal transduction occurs, resulting in heat generation. This heat energy is used to destroy cancer cells as cell viability is compromised when the temperature exceeds 42 °C.[11]

The pioneering work in photothermal therapy using silica–gold/core–shell nanostructures was started by Halas and co-workers.[12] It was shown that by tuning the thickness of the shell, the SPR absorption can be shifted to desired wavelengths. El sayed and co-workers[13] showed that gold nanorods can also be used for PTT when their longitudinal SPR absorption is tuned to the NIR region. Halas and co-workers[14] have compared the photothermal efficiencies of nanoshells and nanorods. They have found that the gold nanorods and Au/Au_2S nanoshells have better photothermal transduction efficiencies than the Au/SiO_2 nanoshells. Wang et al.[15] have compared the photothermal efficacy of gold nanohexapods with gold nanorods and gold nanocages. The gold nanocages were synthesized as plasmonically active photothermal agent by Chen et al.[7] and Hu et al.[16] Currently, the gold nanostructures are also being researched for their application in controlled release, loading of photosensitizers for photodynamic therapy, and in imaging.[17–20] Khlebtsov et al.[21] reported that among the gold nanostructures, the nanocages were very effective in photothermal conversion in comparison to nanoshells and nanorods. But their photothermal efficiency in cancer cell lines was not compared. Cheng et al.[22] have compared nanoshells with nanorods for their photothermal efficiency in cancer cell lines, but nanocages were not included in their analysis. Though all of these gold nanostructures were tested individually for their effectiveness in various cancer cell lines, the size of each nanostructure, the cell lines used, the laser power used, etc., were not same in

© 2013 WILEY-VCH Verlag GmbH & Co. KGaA, Weinheim

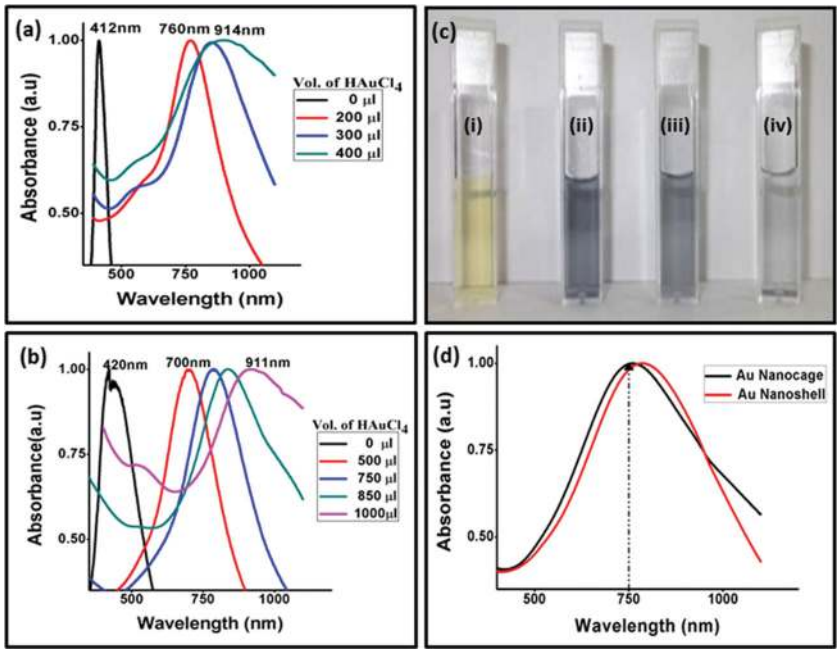

Figure 1. UV–vis absorbance of a) Gold nanocages, b) Gold nanoshell; c-i) Image of silver nanocube solution (412 nm wavelength of absorbance); c-ii,iii,iv) Images of gold nanocage solutions that were formed by galvanic replacement of silver nanocubes with varying amount of 1×10^{-3} M $HAuCl_4$ c-ii) 200 µL (760 nm) c-iii) 300 µL (850 nm) and c-iv) 400 µL $HAuCl_4$ (914 nm) respectively; d) Absorbance of the sample solution of gold nanocages and gold nanoshells that were taken up for further characterization and experimental analysis—both having absorbance at around 750 nm wavelength.

each of these studies.[7,13,23] Recently, Bartczak et al.[24,25] have studied the interaction of various gold nanostructures (that are plasmonically active) with human endothelial cells. But their interaction with tumorigenic cell line like MDA MB 231 is yet to be analyzed. Hence, a comparative analysis of gold nanocages with that of the gold nanoshells under similar conditions is warranted.

In the current study, we have compared gold nanocages with hollow gold nanoshells (henceforth referred to as gold nanoshells) under similar conditions, using continuous wave NIR laser (750 nm) with fixed power (650 mW). The comparison was performed in terms of photothermal efficiency, biocompatibility with normal cell lines (L929 – mouse fibroblast) and photothermal ablation of breast cancer cell line (MDA-MB-231). Both qualitative and quantitative analyses of PTT using gold nanocages and gold nanoshells were conducted. It was observed that under in vitro conditions, the gold nanocages exhibit higher efficiency than gold nanoshells in photothermal-mediated cell cytotoxicity leading us to believe that these nanocages may find use in vivo.

2. Results and Discussion

2.1. NIR Absorbance

Au nanocages were prepared by galvanic replacement of silver nanocubes.[26] The silver nanocubes gave an absorbance peak at 412 nm. As the titration reaction proceeds, the wavelength corresponding to nanocage formation begins to emerge with a red shift. For 0.2 mL of $HAuCl_4$ solution, the wavelength was around 760 nm. Subsequently with 0.3 mL of $HAuCl_4$, peak absorbance wavelength was shifted to 850 nm. With 0.4 mL of $HAuCl_4$, the wavelength was further shifted to 914 nm. This red shift is clearly depicted in **Figure 1**a. This SPR change could be visualized during the course of the reaction as the color changes from yellow to dark blue. When almost all the silver got replaced by gold deposition, the solution turned to light blue in color (Figure 1c). Xia et al. had earlier reported the formation of pinholes in the nanocages prepared by galvanic replacement route. We have also confirmed the formation of such pinholes (**Figure 2**d, red arrows). It is through these pinholes that the silver ions get evacuated from the template. For the nanoshells, the silver nanosphere templates gave an absorbance peak at 420 nm, but as the titration reaction continues, the wavelength corresponding to gold nanoshells begin to emerge with a red shift. For 0.5 mL of $HAuCl_4$, the wavelength shifted to 700 nm. Subsequently with 0.75 mL of $HAuCl_4$, wavelength was further shifted to 785 nm. With 1 mL of $HAuCl_4$, wavelength peaked at 911 nm (Figure 1b). The wavelengths of both gold nanocages and gold nanoshells were tuned to around 750 nm by optimizing the amount of $HAuCl_4$ added to the silver template solution (Figure 1d). These samples (which were pre-tuned to 750 nm absorbance) were then taken up for further characterization studies and cell culture experiments.

2.2. Characterization of Gold Nanostructures

Dynamic light scattering (DLS) was performed to understand the size distribution and polydispersity of the gold

© 2013 WILEY-VCH Verlag GmbH & Co. KGaA, Weinheim
Part. Part. Syst. Charact. **2013**,
DOI: 10.1002/ppsc.201300173

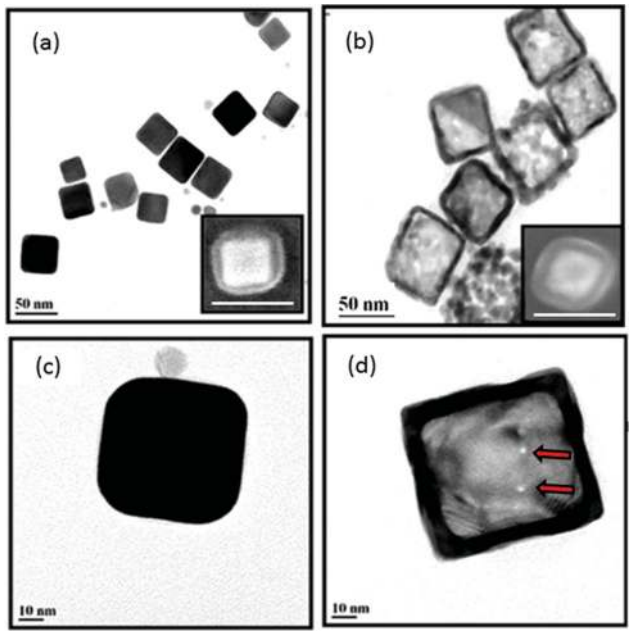

Figure 2. TEM images of silver nanocubes and gold nanocages. a) Silver nanocubes (inset-SEM image of a silver nanocube with scale bar –50 nm). b) Gold nanocages (inset-SEM image of a gold nanocage with scale bar –50 nm), c) TEM image of a typical silver nanocube (412 nm absorbance), d) a typical gold nanocage (750 nm absorbance) showing pinholes (red arrows).

nanostructures. The gold nanocages had a hydrodynamic diameter of 48.7 ± 5.27 nm with a polydispersity index of 0.21 (Figure S1, Supporting Information). The zeta potential of the Ag nanocubes (template) was neutral and that of the Au nanocages was tending towards negative (–13.64 ± 0.86 mV). field emission gub–transmission electron microscopy (FEG-TEM) showed the size of gold-nanocages to be around 30–40 nm edge length as shown in Figure 2b. The clear change in the contrast between Ag nanocubes and Au nanocages is an indication that the replacement reaction has taken place successfully (Figure 2a,b). This replacement process became more evident when varying amounts of $HAuCl_4$ (1×10^{-3} M) were added to the Ag nanocubes solution (Figure S1-c, Supporting Information). FEG-scanning electron microscopy (SEM) showed the surface morphology to be smooth and size of gold nanocage was similar to that seen on TEM (Figure 2a,b insets). X-ray diffraction (XRD) analysis of the silver nanocubes revealed peaks at (111),(200),(220) and (311) corresponding to face centered cubic (FCC) structure. Also, the increasing concentration of sodium sulphide showed a corresponding increase in (200), i.e., equivalent of (100) peak, with respect to the (111) peak denoting the high yield of nanocubes which form templates for nanocages (**Figure 3**a–d). We have observed that only for an optimal concentration of Na_2S (100 µL of 3×10^{-3} M), the yield of Ag cubes was high. We had varied the concentration of Na_2S by increasing the volume of 3×10–3 M solution from 50 to 150 µL. It was noted that only for 100 µL sample solution, the XRD peak of the flat cubic facets, i.e., (200) became prominent whereas for the other concentrations (i.e., 50 and 150 µL of 3×10^{-3} M Na_2S) the peak was not significantly high (Figure S2, Supporting Information). A line-scan was performed on both the Ag cube and the Au cage. The reduction of Ag content in the center region and the thin deposition of Au onto the surface was also confirmed as shown in Figure 3e,f. The size of the gold nanoshells was found to be around 40–60 nm, as shown in TEM and SEM analysis (**Figure 4**b). The size range was similar in DLS analysis as well and was observed to be around 64.5 ± 4.33 nm. The polydispersity index was 0.214 (Figure S1, Supporting Information). The zeta potential of the Ag nanospheres was also neutral, like that of the Ag nanocubes. The gold nanoshells had a zeta potential of –11.81 ± 1.85 mV. Both the gold nanocages and nanoshells were quite stable owing to the poly(vinyl pyrrolidone) (PVP) surface coating that provided the necessary steric hindrance to the neighboring particles. PVP has been considered to be better than poly ethylene glycol (PEG) in evading accelerated blood clearance (ABC).[27] Hence, the PVP-coated gold nanocages and nanoshells were further subjected to experimental analysis without pegylation.

We observed that for different concentration ranges of the bare nanostructure sol. that have absorbance around 750 nm wavelength, the absorption intensity of nanocages slightly exceeded the nanoshells. When a linear fit was analyzed by plotting absorbance at different mass ranges, the slope, i.e., the coefficient of extinction per unit mass for the gold nanocages slightly exceeded the gold nanoshells by a narrow range. The coefficient of extinction per unit mass for the gold nanocages was 0.116 ± 0.0019 and for that of the gold nanoshells was 0.0995 ± 0.0015 (**Figure 5**a). Inductively coupled plasma–atomic emission spectroscopy (ICP-AES) was performed to determine the silver and gold concentration in Ag template solutions (i.e., Ag nanospheres and Ag nanocubes), gold nanocage and nanoshell solutions. In the ICP-AES study of bare gold nanoshells sol. (750 nm absorbance), the concentration of silver was equivalent to that of gold concentration, whereas in the case of bare gold nanocages sol. (750 nm absorbance), the concentration of silver was very much less than the gold concentration. Also, the galvanic replacement reaction was confirmed by the reduction of silver concentration in comparison to the template solutions (Figure S3, Supporting Information). The ICP-AES-based cell uptake of gold nanostructures by breast cancer cells (MDA MB 231) revealed that the gold nanocages were taken up at a concentration (77.73 ± 6.5%) comparable to that of the gold nanoshells (69.8 ± 0.93%), indicating that almost equal amount of elemental gold percentage from gold nanocages (100 µg mL^{-1}) and gold nanoshells (100 µg mL^{-1}) were imbibed by the cancer cells (Figure 5b). The subtle difference in the uptake percentage could have been due to cell death owing to the presence of silver in the gold nanoshells that were not replaced by gold. Also, considering the similarity in uptake percentage and the extinction coefficient per unit mass of the gold nanocages and nanoshells, it is observed that there could not be a significant difference in the number of photothermally active particles taken up by the cancer cells.

The aim of the study was to compare the photothermal properties of gold nanocages and gold nanoshells at a specific NIR wavelength (650–900 nm). At wavelengths higher than 900 nm, the galvanic replacement of silver by gold will be completed, and the entire structure will break down into gold particles owing to loss of template structure. At wavelengths lesser

© 2013 WILEY-VCH Verlag GmbH & Co. KGaA, Weinheim

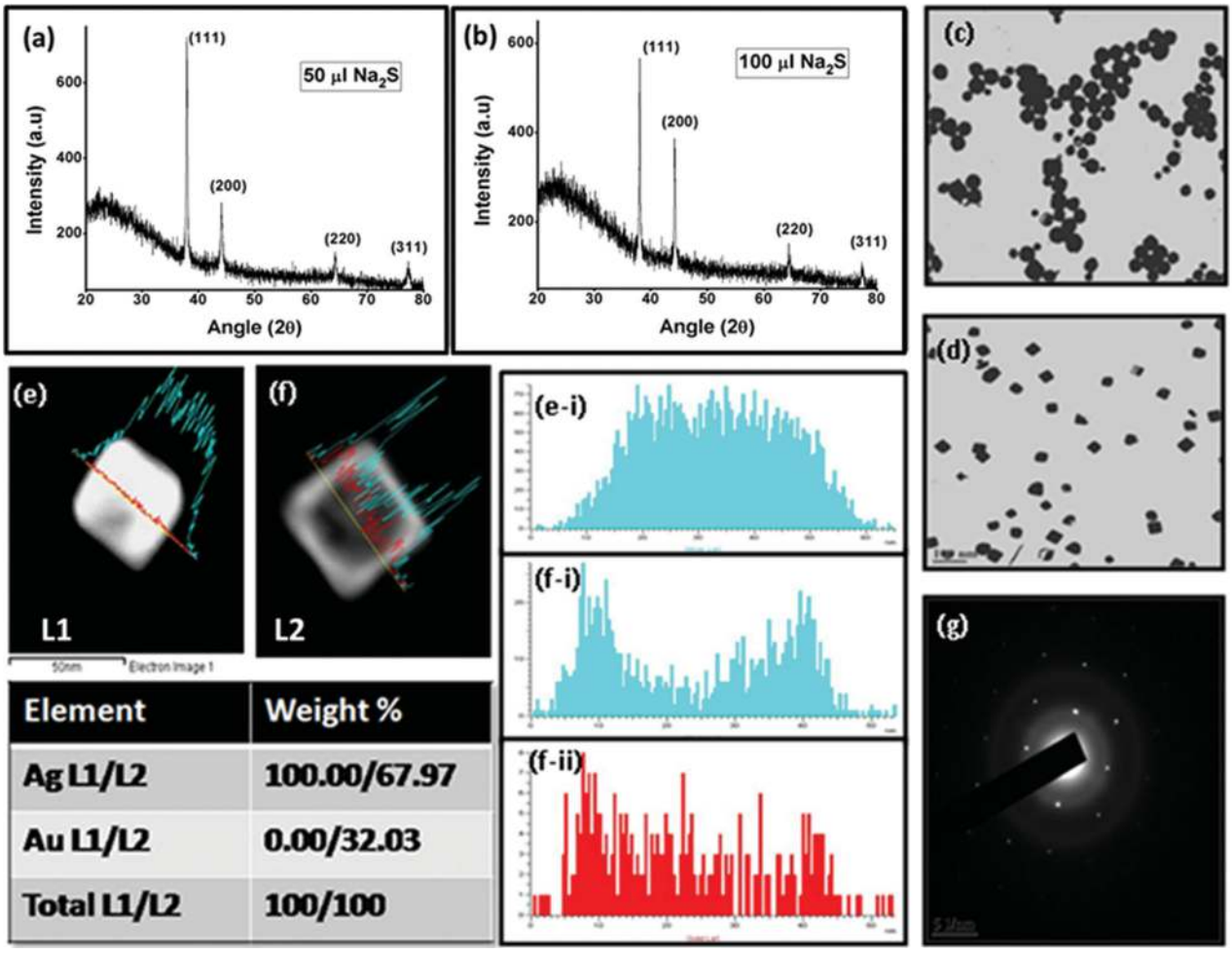

Figure 3. XRD of silver nanoparticles with a) 50 µl Na_2S, b) 100 µL Na_2S. TEM images of silver nanoparticles corresponding to XRD, c) with 50 µL Na_2S, d) with 100 µL Na_2S, e) Line scan of silver nanocube – L1, f) Line scan of gold nanocage – L2, e-i) graph of Ag distribution in silver nanocube, f-i) graph of Ag distribution in gold nanocage, f-ii) Graph of Au distribution in gold nanocage, g) Diffraction pattern of a typical gold nanocage corresponding to (100) lattice pattern.

than 650 nm, the replacement reaction would be incomplete, and such structures would not be appropriate for photothermal therapy. Hence, a 750 nm NIR wavelength was chosen for further experimental analysis. The photothermal-mediated temperature rise experiment was performed for the gold nanocages using a 750 nm infrared laser source. The experimental set up has been shown in the Figure S4 (Supporting Information). The solution temperature was measured before switching on the laser set-up. This initial temperature corresponds to the lab temperature at the time of performing the study, which was measured to be 24 °C. Water was taken as the control to eliminate the heat produced by the laser source. As shown in Figure 5c, it was observed that the temperature began to rise immediately as the laser was switched on. There was a 20 °C increase observed in the nanocage solution in 10 min, and the temperature then stabilized to a 24 °C increase at the end of 20 min. In the case of nanoshells as well, it was observed that the temperature began to rise immediately as the laser was switched on. There was a 15 °C increase in 10 min, which further stabilized to an 18 °C increase at the end of 20 min. As the nanoparticle solutions were irradiated with NIR laser, they began to absorb NIR light owing to their surface plasmon resonance, which in turn was responsible for rapid heat generation. Though the difference between the extinction coefficient per unit mass of nanocages and nanoshells was not very high (see Figure 5a), when extrapolated to higher masses (i.e., 50 µg), such subtle differences could lead to significant changes in photothermal heat conversion. The photothermal-mediated temperature rise experiment proved that the gold nanocages were very effective in photothermal conversion in comparison to the gold nanoshells. The gold nanoshells solution subjected to laser treatment was able to reach 40–41 °C at a very rapid phase, but beyond 41 °C the temperature increase was very slow. In the case of the gold nanocage, the temperature increase was very quick and efficient. The solution was able to achieve 43 °C in just 6–8 min. This kind of temperature rise was due to transmittance of localized heat to the surrounding media. In order to cause such high temperature rise in the entire solution, the localized heat generated on the surface should be very high in such a way that it would exceed the melting point of gold nanoparticles as reported by Wu

© 2013 WILEY-VCH Verlag GmbH & Co. KGaA, Weinheim
Part. Part. Syst. Charact. **2013**,
DOI: 10.1002/ppsc.201300173

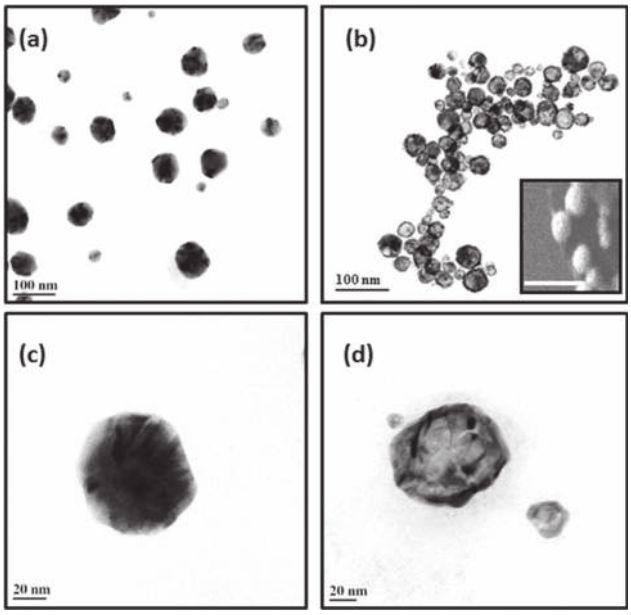

Figure 4. TEM images of a) Silver nanospheres, b) Gold nanoshells (inset: SEM image of gold nanoshells with scale bar 100 nm), c) TEM image of a typical silver nanosphere (420 nm absorbance) and d) a typical gold nanoshell (750 nm absorbance).

et al.[28] We subjected concentrated solution of gold nanocage (5×) to laser treatment, and the effect of localized heat on the nanostructure was analyzed. The SEM and TEM analysis revealed certain bleb formation on the surface of cages, indicating a structural modification that indirectly confirmed the high localized temperature rise that could be achieved by a photothermal effect. The NIR absorbance of the concentrated solution (post-irradiation) significantly decreased reconfirming the structural modification (Figure S5, Supporting Information). Thus, the nanocages when treated with laser emit tremendous amount of localized heat that could facilitate photothermal therapy of cancer cells. There could not be any significant changes identified in the morphology when gold nanoshells were treated with laser. This could be because of the shape of the gold nanoshells. The gold nanoshells were already quasi-spherical in shape with many bleb-like (hemispherical projections) arrangements on the surface. Hence, any changes (such as bleb formation) similar to those of nanocages would be difficult to identify.

2.3. Biocompatibility Studies

Biocompatibility studies were performed using MTT assay in L929 cell line. The toxic effect of the gold nanocages was observed for concentrations ranging from 1 to 100 μg mL^{-1} at the end of a

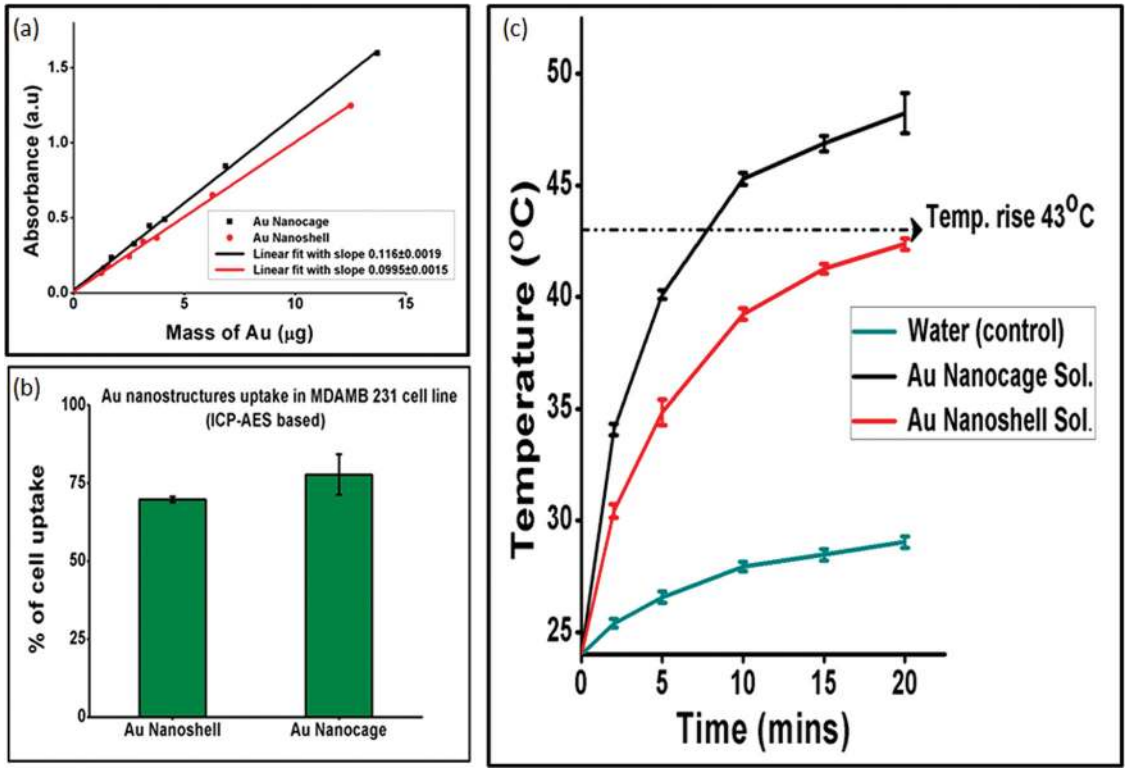

Figure 5. a) Extinction coefficient per unit mass for gold nanocage and gold nanoshell sol. calculated by fitting a linear curve for absorbance intensity measured (at 750 nm) for different mass range of Au in the respective sample solutions. The extinction coefficient per unit mass was found to be 0.116 ± 0.0019 and 0.0995 ± 0.0015 for gold nanocage and gold nanoshell respectively. b) ICP–AES-mediated cell uptake analysis of Au nanostructures by MDA MB 231 cells. Gold nanoshell and gold nanocage sol. with absorbance at 750 nm were incubated with cancer cells for 5 h at Au conc. of 100 μg mL^{-1}. (Number of repeats, $n = 3$) c) Photothermal conversion efficiency of gold nanostructures depicted in terms of temperature rise experiment. For the photothermal experiment, 1 mL of gold nanocage and gold nanoshell sol. (50 μg mL^{-1} Au conc.) having absorbance at 750 nm wavelength were taken up for NIR irradiation. (Number of repeats, $n = 3$).

© 2013 WILEY-VCH Verlag GmbH & Co. KGaA, Weinheim

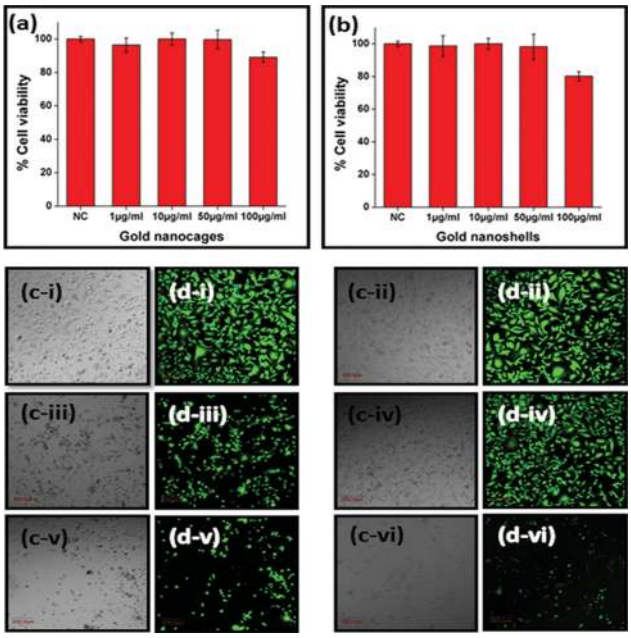

Figure 6. Biocompatiblity studies of a) gold nanocages b) gold nanoshells performed in L929 mouse fibroblast cell line for concentrations ranging from 1 to 100 µg mL^{-1} of Au (MTT Assay). (Number of repeats, $n = 3$), c,d) Qualitative analysis of photothermal cytotoxicity by gold nanostructures in MDA MB 231 cells. c) Differential interference contrast (DIC) images and d) calcein AM- live cell images; c,d-i) no treatment, c,d-ii) laser (750 nm) treatment for only 10 min, c,d-iii) only gold nanoshells, c,d-iv) only gold nanocages, c,d-v) gold nanoshells + laser (10 min), c,d-vi) gold nanocages + laser (10 min).

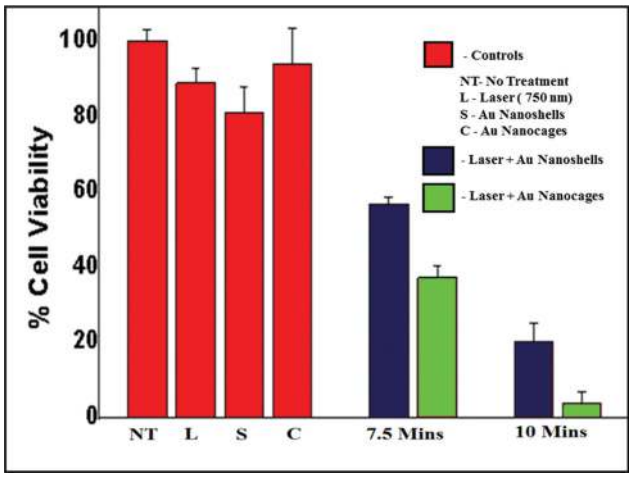

Figure 7. Quantitative analysis (MTT assay) of photothermal cytotoxicity by gold nanostructures in MDA MB 231 breast cancer cells. The controls (red columns) included cancer cells without any treatment (NT), cancer cells irradiated with laser (750 nm) for 10 min (L), cancer cells incubated with gold nanoshells (S) and gold nanocages (C). The test samples (blue and green columns) included cancer cells incubated with gold nanoshells/gold nanocages and then treated with laser for 7.5 and 10 min. Blue columns: laser + gold nanoshells. Green columns: laser + gold nanocages. (Number of repeats, $n = 3$).

24 h incubation period. As shown in **Figure 6**a, the cell viability with the gold nanocages were well above 90% until 100 µg mL^{-1} concentration, indicating that these are very much biocompatible with the physiological system. The toxic effect of the gold nanoshells was also observed for the same concentrations, ranging from 1 µg mL^{-1} to 100 µg mL^{-1} at the end of 24 h incubation period. As shown in Figure 6b, the cell viability with the gold nanoshells were well above 90% till 50 µg mL^{-1} concentration. The cell viability decreased slightly to 80% with 100 µg mL^{-1} concentration. Thus, the gold nanoshells as well were quite biocompatible having only little cytotoxic effect even at 100 µg mL^{-1} concentration. As discussed earlier, the insignificantly low cytotoxic effect shown by the gold nanoshells could be attributed to the presence of silver in the particles that were not replaced by gold.

2.4. Photothermal Therapy in Cancer Cells

The laser-mediated photothermal ablation experiment was performed in MDA-MB 231 breast cancer cell line grown in 96-well plates. The particles (gold nanocages and gold nanoshells with 750 nm absorbance) were compared for 100 µg mL^{-1} gold concentration. After 5 h of incubation at 37 °C, the unbound particles were removed by PBS wash (thrice) and then subjected to laser treatment (750 nm laser, 650 mW, continuous wave). It was observed that when the cells were treated with laser for 7.5 min, the cell death was 62.92 ± 3.25% in the case of gold nanocages and 43.35 ± 1.91% in gold nanoshells (MTT assay). When treated for 10 min with laser, almost all of the cells were dead in the well plate incubated with gold nanocages (96.41 ± 3.04% cell death) and 79.89 ± 4.74% cell death was observed in the case of gold nanoshells (**Figure 7**). In the qualitative analysis as well, the same trend was observed with the gold nanocages showing higher efficiency in photothermal cell death in comparison to the gold nanoshells (Figure 6c,d). Even with 5 min of laser irradiation, the formation of apoptotic bodies was observed from live cells that were treated with gold nanocages and laser (white arrows, **Figure 8**b). At the end of 10 min, most of the cells died, which was evident by PI staining (Figure 8c).

The qualitative analysis (calcein AM live cell imaging) and the quantitative analysis (MTT assay) proved that the gold nanocages were very effective in absorbing NIR laser and mediating photothermal-facilitated cancer cell death in MDA-MB 231 cell lines (breast cancer cell line). After the cells die, they cannot convert calcein-AM to calcein (fluorophore). Hence, significant reduction in density of green fluorescence indicating cancer cell death was observed in well plates (incubated with gold nanocages) that had undergone NIR laser irradiation (Figure 6c,d). The cancer cells incubated with gold nanoshells followed by NIR laser irradiation also showed qualitative and quantitative reduction in cell viability. But the gold nanocage-mediated photothermal cytotoxicity was superior to that of the gold nanoshells both for 7.5 min as well as 10 min of NIR laser irradiation (Figure 7). In the individual controls, i.e., the well plates with no treatment, only laser and only particles (i.e., gold nanocages and gold nanoshells), no significant reduction in cell viability was noted. Hence, the cell death that occurred could very well be attributed to photothermal effect that aided in increasing the temperature of the cancer cells to incompatible level. The dead cell staining (PI) performed immediately

© 2013 WILEY-VCH Verlag GmbH & Co. KGaA, Weinheim

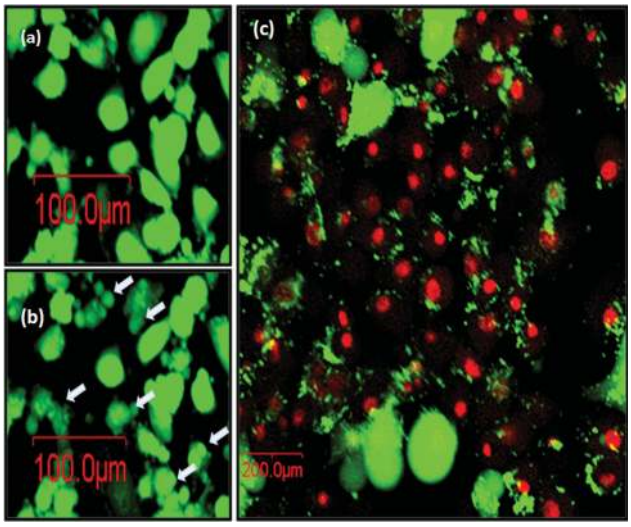

Figure 8. MDA MB-231 cells (calcein and PI-stained) treated with gold nanocages and NIR laser a) 0 min laser irradiation, b) 5 min laser irradiation showing formation of apoptotic bodies (white arrows), c) 10 min laser irradiation showing formation of PI-stained dead cells.

after laser treatment enabled us to observe the formation of dead cells among few live cells that were incubated with gold nanocages (100 µg mL^{-1}), thus confirming photothermal effect (Figure 8c). The gold nanocages showed better photothermal conversion efficiency and better biocompatibility in comparison to the gold nanoshells, when all of the important parameters were kept constant (concentration, laser power, and irradiation time). In the in vitro photothermal-mediated cancer cell cytotoxicity as well, the gold nanocages were able to mediate higher degree of cancer cell death in comparison to gold nanoshells. We observe that the variation between the gold nanocages and gold nanoshells in terms of size, extinction coefficient per unit mass, cellular uptake, and biocompatibility, though subtle on individual basis, all have a synergistic role in achieving a significant difference in terms of in vitro photothermal cytotoxicity.

3. Conclusion

The gold nanocages were observed to be highly efficient photothermal converting agents, faster than gold nanoshells in increasing the temperature of the surrounding media. They were also found to be very much biocompatible when treated with normal cell lines even at high concentration (100 µg mL^{-1} of gold). When subjected to laser-mediated cancer cell cytotoxicity, the gold nanocages turned out to be better agents in inducing cell death more effectively than their counterpart. Therefore, considering all the essential criteria, i.e., in terms of size, biocompatibility, photothermal conversion, and laser-mediated cancer cell cytotoxicity, the gold nanocage system appears to be a preferable one for PTT when compared with the gold nanoshells. Further, the differences in the pharmacokinetics, bio-distribution, physiological clearance, and PTT efficiency of these gold nanostructures in the in vivo conditions have to be analyzed. This will enable us to understand and choose the best among the available nanosystems for PTT of cancer.

4. Experimental Section

Materials: Tetrachloroauric acid trihydrate ($HAuCl_4 \cdot 3H_2O$) and silver nitrate ($AgNO_3$) were purchased from Acros Organics (Thermo Fisher Scientific Inc.). Polyvinyl pyrrolidone (PVP) and sodium sulphide (55%) were purchased from Merk. L-Ascorbic acid (AA), methyl tetrazolium salt (MTT), propidium iodide (PI), and calcein-AM were purchased from Sigma-Aldrich, USA. Sterile phosphate buffer saline (PBS), Dulbecco's minimal essential media (DMEM), fetal bovine serum (FBS), and trypsin–ethylene diamine tetra-acetic acid (EDTA) were purchased from Himedia Lab, India. All other reagents were purchased from Spectrochem India Pvt. Ltd. All chemicals were reagent grade and used as received. All glasswares were cleaned with freshly prepared aqua-regia and rinsed with water before use. Ultra-pure de-ionized water (Milli Q) was used for all solution preparations and experiments.

Synthesis of Gold Nanocages: Gold nanocages were synthesized according to the method of Siekkinen et al.[26] with slight modification. In a typical synthesis, 6 mL ethylene glycol was heated under stirring with a teflon-coated magnetic stirring bar for 1 h in a 25-mL conical glass vial. While the ethylene glycol (EG) was heated, EG solutions containing $AgNO_3$ (50 mg mL^{-1}) and PVP (25 mg mL^{-1}) were prepared. A 3×10^{-3} M solution of Na_2S in EG was freshly prepared and 100 µL of the sulfide solution was injected into the conical flask containing EG PVP (2 mL) and $AgNO_3$ (0.5 mL) solutions were sequentially injected. As silver nitrate was added, the colorless solution turned bright yellow. The appearance of yellow color indicates the formation of small silver particles. After 5–10 min into the reaction, the solution darkened to an orange–yellow color. After 15–20 min, the solution changed color to an opalescent ruddy-brown and concurrently became opaque. If allowed to continue, the solution faded to a lighter, whitish–brown color but remained opaque. The reaction was stopped at the end of 45 min.

A fixed amount (200 µL) of the as-synthesized silver nanocubes was dispersed in 5 mL water containing 1 mg mL^{-1} PVP in a 25-mL flask under magnetic stirring and then heated to boil for 10 min. A specific amount (0.2–0.4 mL) of 1×10^{-3} M $HAuCl_4$ aqueous solution was added to the flask through a syringe pump at a rate of 40 mL h^{-1} under magnetic stirring. The solution was heated for another 10 min until the color of the system was stable. Once cooled down to room temperature, the sample was centrifuged and washed with saturated NaCl solution to remove AgCl and then with water several times to remove PVP and NaCl before characterization by TEM and SEM.

Synthesis of Gold Nanoshells: Gold nanoshells were synthesized by galvanic replacement reaction, wherein an initial template structure (silver nanoparticles) was prepared followed by replacement reaction with gold.[29] For the synthesis of silver nanoparticles with a quasi-spherical shape, 0.025 g of $AgNO_3$ and 0.10 g of PVP were dissolved in 10 mL of ethylene glycol. This mixture was then heated at 160 °C for 1.5 h under vigorous magnetic stirring. In a typical procedure, a 250 µL aliquot of the as-obtained dispersion of silver nanoparticles was added to 5 mL of deionized water. The solution was heated to 150 °C for 10 min. This was followed by titration reaction using 1×10^{-3} M $HAuCl_4$. As the $HAuCl_4$ was added drop by drop, a corresponding change in the color of the solution was noted. The solution finally changes to bluish violet color, which is then cooled to room temperature before further characterization.

Characterization of Gold Nanostructures: The size and polydispersity of gold nanocages and gold nanoshells were measured using DLS device (Brookhaven Instruments, USA). Zeta potential was analyzed using a Brookhaven zeta potential analyser. UV–vis spectral analysis of gold nanostructures (cages and shells) was performed using a Perkin Elmer (Lambda 25) instrument. SEM (JSM-7600F) and TEM (JEM-2100 F-JEOL and Philips CM200) of silver and gold nanostructures were also performed. In a typical TEM/SEM sample preparation, 10 µL (three times dilution) of the sample was drop casted on a copper grid/stub and allowed to air-dry for 48 h. Percentage element analysis was also performed for silver nanoparticles and gold nanostructures using energy dispersive X-ray spectroscopy (OXFORD – EDX). Elemental analysis of gold and silver was performed using ICP-AES (ARCOS, Germany, detection limit of 0.01 PPM). In a typical sample preparation process for

© 2013 WILEY-VCH Verlag GmbH & Co. KGaA, Weinheim

ICP-AES analysis, 200 µL of the sample was dissolved in 1 mL of freshly prepared aqua regia and then diluted to 12 mL with distilled water. This diluted sample was subjected to gold and silver quantification.

Photothermal Studies: Photothermal effect of the prepared nanostructures was studied with the help of 750 nm NIR laser (650 mW-PMC, India). In a typical experiment, 1 mL of the prepared solutions (gold nanocages and gold nanoshells at 50 µg mL^{-1} gold concentration) were taken in a 4-mL glass cuvette and mounted on a stand inside a sealed box. A laser is allowed to pass through the side walls of the cuvette in such a way that it covers the filled solution from one end to the other. Simultaneously, the rise in temperature was recorded with the help of a digital thermometer (thermocouple type). The temperature was recorded at 0, 2, 5, 10, 15, 20 min, respectively. All of the experiments were conducted at 24 °C, and the subsequent rise in temperature was plotted as an increment from baseline.

In Vitro Biocompatibility Studies: In vitro biocompatibility studies were done using the MTT assay in L929 cell line. Exponentially growing cells were dispensed into a 96-well flat bottom plate at a concentration of 1×10^5 cells $well^{-1}$. After allowing 24 h for cell attachment, gold nanostructure solutions were diluted appropriately in fresh media and added (200 µL) in the concentration ranging from 1 to 100 µg mL^{-1} (three wells per sample concentration). The media was not changed during the incubation of 24 h. Following incubation, cell viability was determined by the addition of MTT (20 mL, 5 mg mL^{-1} dye in sterile PBS). The plate was incubated for an additional 4 h at 37 °C and 5% CO_2, allowing viable cells to convert the pale yellow MTT to an insoluble purple dye. The media were carefully removed and the dye was dissolved in isopropyl alcohol (200 µL). Absorbance values at 595 nm were collected and cell viability was calculated as a percentage compared with untreated control cells.

In Vitro ICP-Mediated Cell Uptake Studies: MDA-MB-231 cells were seeded onto a 96-well plate with a density of 1×10^4 cells per well. Cells were washed three times with PBS the following day, and then the cells were incubated with particles (gold nanocages and gold nanoshells) at 37 °C for 5 h (100 µg mL^{-1} gold concentration) Thereafter, cells were washed three times with PBS to remove unbound particles. Cells were then trypsinized by adding 40 µL trypsin EDTA. These trypsinized cells containing gold nanostructures were then dissolved in freshly prepared aqua regia (1 mL) and made upto 12 mL by diluting with MilliQ water. They were then subjected to ICP–AES analysis to understand the percentage of elemental gold take up by the cancer cells.

In Vitro Laser-Mediated Photothermal Ablation of Tumor Cells: MDA-MB-231 cells were seeded onto a 96-well plate with a density of 1×10^4 cells per well 1 d before the irradiation experiment. Cells were washed three times with PBS. The following order of treatment was performed: no treatment, NIR laser alone (10 min irradiation), gold nanoshells alone, gold nanocages alone, gold nanoshells with laser (7.5 and 10 min irradiation) and gold nanocages with laser (7.5 and 10 min irradiation). For treatment with nanocages and nanoshells, cells were incubated with particles (gold nanocages and gold nanoshells) at 37 °C for 5 h (100 µg mL^{-1} gold concentration). Thereafter, cells were washed three times with PBS to remove unbound particles. Cells were then resupplied with DMEM containing 10% FBS. Cells were irradiated with NIR laser (750 nm) and then incubated at 37 °C for 12 h. Then, the cells were washed with PBS and subjected to MTT analysis. For qualitative examination, 24 well plates were used, which were seeded with a density of 1×10^5 cells per well. The remaining protocol was similar to one followed for the above MTT assay, except that at the end of 12 h incubation, cells were washed with PBS and stained with calcein AM (for visualization of live cells) and propidium iodide (for visualization of dead cells). Cells were examined using Olympus model IX81 laser scanning confocal microscope equipped with filters set for excitation/emission wavelengths at 494/517 nm for calcein and 488/617 nm for propidium iodide.

Supporting Information

Supporting Information is available from the Wiley Online Library or from the author.

Acknowledgements

The authors acknowledge Ms. Megha Sanyal for performing biocompatibility studies at NCCS, Pune, "DBT – Nanomedicine" for funding the project, Centre for Research in Nano Technology and Science (CRNTS) and Sophisticated Analytical Instruments Facility (SAIF), IIT Bombay, for the facilities provided for characterization studies.

Received: April 30, 2013
Revised: August 13, 2013
Published online:

[1] P. Alivisatos, *Nat. Biotechnol.* **2004**, *22*, 47.
[2] C. Loo, A. Lowery, N. Halas, J. West, R. Drezek, *Nano Lett.* **2005**, *5*, 709.
[3] M. Hu, J. Chen, Z.-Y. Li, L. Au, G. V Hartland, X. Li, M. Marquez, Y. Xia, *Chem. Soc. Rev.* **2006**, *35*, 1084.
[4] D. Pissuwan, S. M. Valenzuela, M. B. Cortie, *Trends Biotechnol.* **2006**, *24*, 62.
[5] D. A. Giljohann, D. S. Seferos, W. L. Daniel, M. D. Massich, P. C. Patel, C. A. Mirkin, *Angew. Chem. Int. Ed. Engl.* **2010**, *49*, 3280.
[6] M. E. Stewart, C. R. Anderton, L. B. Thompson, J. Maria, S. K. Gray, J. A. Rogers, R. G. Nuzzo, *Chem. Rev.* **2008**, *108*, 494.
[7] J. Chen, D. Wang, J. Xi, L. Au, A. Siekkinen, A. Warsen, Z.-Y. Li, H. Zhang, Y. Xia, X. Li, *Nano Lett.* **2007**, *7*, 1318.
[8] N. G. Khlebtsov, L. A. Dykman, *J. Quant. Spectrosc. Radiat.Transf.* **2010**, *111*, 1.
[9] N. Rozanova, J. Zhang, *Sci. China, Ser. B, Chem.* **2009**, *52*, 1559.
[10] B. P. Timko, T. Dvir, D. S. Kohane, *Adv. Mater.* **2010**, *22*, 4925.
[11] B. V. Harmon, Y. S. Takano, C. M. Winterford, G. C. Gobe, *Int. J. Radiat. Biol.* **1991**, *59*, 489.
[12] S. J. Oldenburg, J. B. Jackson, S. L. Westcott, N. J. Halas, *Appl. Phys. Lett.* **1999**, *75*, 2897.
[13] X. Huang, I. H. El-Sayed, W. Qian, M. A. El-Sayed, *J. Am. Chem. Soc.* **2006**, *128*, 2115.
[14] J. R. Cole, N. A. Mirin, M. W. Knight, G. P. Goodrich, N. J. Halas, *J. Phys. Chem. C* **2009**, *113*, 12090.
[15] Y. Wang, K. C. L. Black, H. Luehmann, W. Li, Y. Zhang, X. Cai, D. Wan, S.-Y. Liu, M. Li, P. Kim, Z.-Y. Li, L. V Wang, Y. Liu, Y. Xia, *ACS Nano* **2013**, *7*, 2068.
[16] M. Hu, H. Petrova, J. Chen, J. M. McLellan, A. R. Siekkinen, M. Marquez, X. Li, Y. Xia, G. V Hartland, *J. Phys. Chem. B* **2006**, *110*, 1520.
[17] M. S. Yavuz, Y. Cheng, J. Chen, C. M. Cobley, Q. Zhang, M. Rycenga, J. Xie, C. Kim, K. H. Song, A. G. Schwartz, L. V Wang, Y. Xia, *Nat. Mater.* **2009**, *8*, 935.
[18] L. Gao, J. Fei, J. Zhao, H. Li, Y. Cui, J. Li, *ACS Nano* **2012**, *6*, 8030.
[19] T. Zhao, X. Shen, L. Li, Z. Guan, N. Gao, P. Yuan, S. Q. Yao, Q.-H. Xu, G. Q. Xu, *Nanoscale* **2012**, *4*, 7712.
[20] X. Xia, Y. Xia, *Front. Phys.* DOI:10.1007/s11467-013-0318-8.
[21] B. N. Khlebtsov, V. A. Khanadeev, I. L. Maksimova, G. S. Terentyuk, N. G. Khlebtsov, *Nanotechnol. Russia* **2010**, *5*, 454.
[22] F.-Y. Cheng, C.-T. Chen, C.-S. Yeh, *Nanotechnology* **2009**, *20*, 425104.
[23] L. R. Hirsch, R. J. Stafford, J. A. Bankson, S. R. Sershen, B. Rivera, R. E. Price, J. D. Hazle, N. J. Halas, J. L. West, *Proc. Natl. Acad. Sci. USA* **2003**, *100*, 13549.
[24] D. Bartczak, O. L. Muskens, S. Nitti, T. M. Millar, A. G. Kanaras, *Small* **2011**, *8*, 122.
[25] D. Bartczak, O. L. Muskens, T. M. Millar, T. Sanchez-Elsner, A. G. Kanaras, *Nano Lett.* **2011**, *11*, 1358.
[26] A. R. Siekkinen, J. M. Mclellan, J. Chen, Y. Xia, *Chem. Phys. Lett.* **2006**, *432*, 491.
[27] T. Ishihara, T. Maeda, H. Sakamoto, N. Takasaki, M. Shigyo, T. Ishida, H. Kiwada, Y. Mizushima, T. Mizushima, *Biomacromolecules* **2010**, *11*, 2700.
[28] G. Wu, A. Mikhailovsky, H. A. Khant, C. Fu, W. Chiu, J. A. Zasadzinski, *J. Am. Chem. Soc.* **2008**, *130*, 8175.
[29] Y. Sun, Y. Xia, *J. Am. Chem. Soc.* **2004**, *126*, 3892.

© 2013 WILEY-VCH Verlag GmbH & Co. KGaA, Weinheim